Cold galaxies *

Michael Rowan-Robinson[1], David L. Clements[1]

†, 1*Astrophysics Group, Imperial College London, Blackett Laboratory, Prince Consort Road, London SW7 2AZ, UK*

3 August 2015

ABSTRACT

We use 350 μm angular diameter estimates from *Planck* to test the idea that some galaxies contain exceptionally cold (10-13 K) dust, since colder dust implies a lower surface brightness radiation field illuminating the dust, and hence a greater physical extent for a given luminosity. The galaxies identified from their spectral energy distributions as containing cold dust do indeed show the expected larger 350 μm diameters. For a few cold dust galaxies where *Herschel* data are available we are able to use submillimetre maps or surface brightness profiles to locate the cold dust, which as expected generally lies outside the optical galaxy.

Key words: infrared: galaxies - galaxies: evolution - star:formation - galaxies: starburst - cosmology: observations

1 INTRODUCTION

One of the surprising results from submillimetre surveys with *Herschel* and *Planck* has been the discovery that some local (z<0.1) quiescent galaxies show spectral energy distributions (SEDs) characteristic of cold (T=10-13 K) dust (Rowan-Robinson et al 2011, 2014, Ade et al 2011, Wang and Rowan-Robinson 2014). Two examples are illustrated in Fig 1.

Cold dust in submillimetre galaxies has also been investigated by Galametz et al (2012), Smith et al (2012) and Symeonidis et al (2013) using SED fitting, by Bourne et al (2013) using CO and by Ibar et al (2013) using CII. Bendo et al (2014) have used surface brightness ratios at 250, 350 and 500 μm to explore the relative contribution of newly formed and old stars to dust heating.

To test the idea that exceptionally cold dust is present in some galaxies we compare *Planck* 350 μm diameters with diameters estimated from radiative transfer models for the far infrared and submillimetre emission. We also look at submillimetre maps for selected galaxies derived from *Herschel* data. Broadly speaking we expect to find that galaxies with colder dust will be more extended spatially at submillimetre wavelengths than normal galaxies of the same luminosity.

The structure of this paper is as follows: in section 2 we estimate the submillimetre diameters for galaxies with cool and cold dust and compare these with predictions for normal cirrus galaxies, in section 3 we compare these predictions

with the 350 μm diameters observed by *Planck* and in section 4 we discuss the few cases where we have *Herschel* maps for cold dust galaxies. Section 5 gives our discussion and conclusions.

2 PREDICTED SUBMILLIMETRE DIAMETERS

The temperature of optically thin interstellar dust ('cirrus') is determined by the intensity of the interstellar radiation field, which can be characterised by the ratio of the intensity of the radiation field to the local Solar Neighbourhood interstellar radiation field, ψ (Rowan-Robinson et al 1992, hereafter RR92). The standard cirrus template of Rowan-Robinson et al (2005, 2008, 2013) corresponds to $\psi = 5$, and this is the value used by RR92 to fit the central regions of our Galaxy. $\psi = 1$ corresponds to the interstellar radiation field in the vicinity of the Sun ('cool' dust). Rowan-Robinson et al (2010, 2014) found that some *Herschel* galaxies need a much lower intensity radiation field than this, with $\psi = 0.1$ ('cold' dust). A similar result was found for some *Planck* galaxies by Ade et al (2011). The corresponding grain temperatures in the dust model of RR92 are given in Table 1 of Rowan-Robinson et al (2010). For the three values of $\psi = 5, 1, 0.1$, the ranges of dust grain temperatures for the different grain types are 20-24 K, 14.5-19.7 K and 9.8-13.4 K respectively. Full details of the templates used are given via a readme page [1].

One of the ways to test these ideas is to measure the

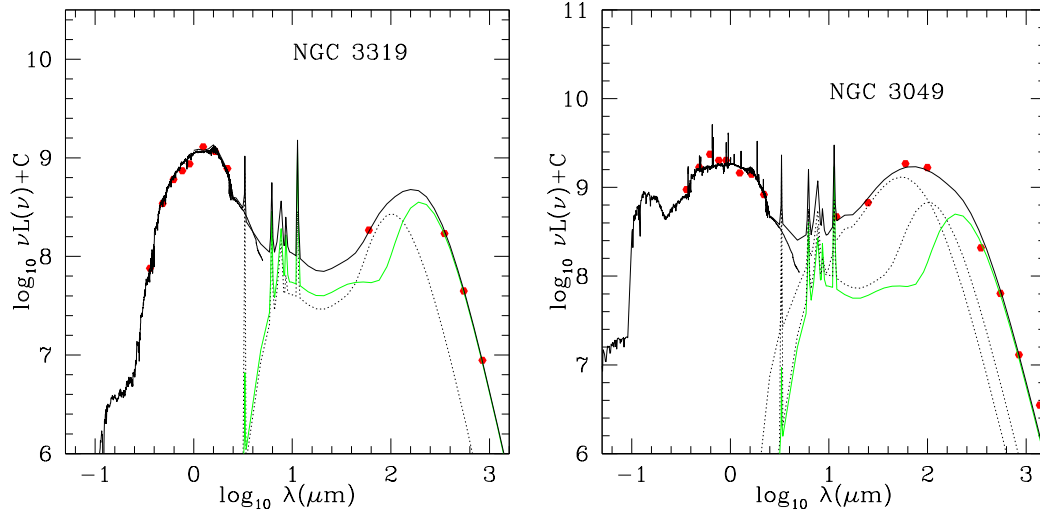[1] http://astro.ic.ac.uk/public/mrr/swirephotzcat/templates/readme

Figure 1. SEDs of NGC 3319 and NGC 3049, showing need for cold dust component (green).
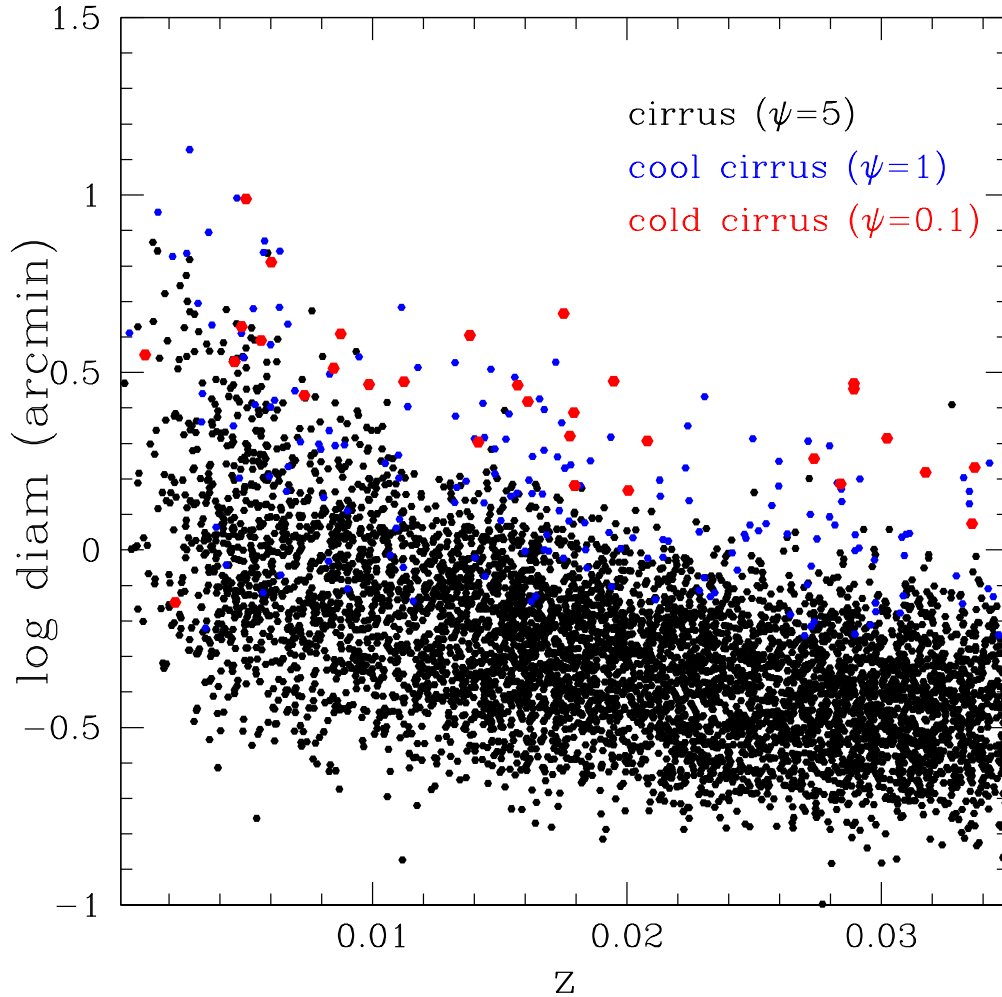

Figure 2. Predicted submillimetre diameter versus redshift for cirrus (ψ=5) galaxies (black), cool galaxies (ψ=1, blue) and cold galaxies (ψ=0.1, red).

submillimetre diameter. Since $\psi = 1$ corresponds to the intensity in the solar neighbourhood, we can estimate the submillimetre diameter of galaxies by

$$\theta \sim 2R_0 \psi^{-0.5} (zc\tau_0)^{-1} (L_{ir}/L_{MW})^{-0.5} \quad (1)$$

where $R_0 = 8.5$ kpc, the distance of the Sun from the Galactic Centre, and $L_{MW} = 2.4.10^{10} L_\odot$. The definition of ψ in the Solar Neighbourhood is in terms of a mean surface brightness and so we can expect that θ defined by this equation is essentially a full-width to half-power when observing external galaxies.

Figure 2 shows a plot of the predicted angular size, θ, versus redshift for galaxies in the RIFSCz IRAS galaxy redshift catalogue (Wang and Rowan-Robinson 2014) whose far infrared and submillimetre emission is best fitted by standard cirrus or cool cirrus, for the sample of *Planck* galaxies identified as requiring cold dust by Ade et al (2011), and for the RIFSCz galaxies identified as needing cold dust templates by Wang and Rowan-Robinson (2014). The prediction is that galaxies with significant cool or cold dust components should have larger submillimetre diameters than their normal cirrus counterparts. Table 1 summarises the properties of the cold dust galaxies from these latter two papers.

3 MEASURED *PLANCK* 350 μM DIAMETERS

We have focussed on those galaxies for which the predicted subillimetre diameter is greater than 3 arcmin and compared these with the PCCS submillimetre diameters (FWHM) observed by *Planck* at 350 μm. We use the Gaussian half-power width measured along the major axis. Table 2 summarises the properties of galaxies from the IRAS RIFSCz catalogue with predicted submillimetre diameter greater than 3 arcmin, spectroscopic redshifts, at least 8 optical photometric bands, χ^2 for the infrared template fit < 5, and SEDs dominated either by a cirrus or cool dust template. Figure 3L shows a comparison of the observed *Planck* diameters with the optical diameters, taken from the 3rd Reference Catalogue of Galaxies, for the galaxies of Tables 1 and 2. The quoted Planck beam at 350 μm is 4.3 arcmin (FWHM), so we deconvolve both the telescope beam and source profile can be approximated as Gaussians. Figure 3R shows a the observed diameters using $\theta_{deconv} = (\theta^2 - 4.3^2)^{-1/2}$, assuming that both the telescope beam and the source profile can be approximated as Gaussians (adaquate for our purposes). Values of $\theta_{deconv} < 4$ arcmin will be subject to considerable uncertainty. Figure 3R shows a comparison of the deconvolved *Planck* diameters with the predicted values from eqn (1). All three types are consistent with a simple linear relation, apart from a cluster of galaxies with anomalously high *Planck* diameters, which we suggest are affected by Galactic cirrus (most have high cirrus flags in the *Planck* PCCS, eg NGC 1024, 3573, 4650, and IC 4831 and 5078). We have fitted straight lines through the origin to these three distributions and find slopes 1.38±0.13 for 40 normal cirrus galaxies, 1.16±0.09 for 64 cool galaxies (excluding 8 probable cirrus sources) and 1.32±0.21 for 8 cold galaxies. Thus all three populations show statistically significant correlations between the observed and predicted diameters, the slopes
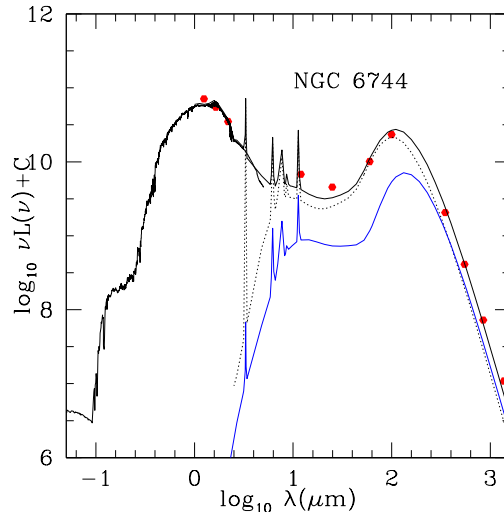

Figure 5. SED of NGC 6744, outlier in Fig 3R.

are consistent with being the same in each case and are also not inconsistent with the true slope being unity.

There are also two outliers with rather large predicted diameters, NGC 6744 and M 104. Figures 4L and 5 show the SEDs for these two outliers. For NGC6744, once the IRAS fluxes from the IRAS Large Galaxy Catalog (Rice et al 1988) have been used, the SED is in fact dominated by a standard cirrus template, so it should move to the left in Fig 3R. For M104, Bendo et al (2006) have suggested that the AGN at the centre of the galaxy contributes to the submillimetre emission. Figure 4R shows *Herschel* 250 μm contours superposed on an i-band image for M104 ('The Sombrero'). The 250 μm emission arises from a ring of dust outside the main distribution of starlight. The predicted value of θ may also be an overestimate because in this edge-on system the starlight illuminating the dust ring has been significantly attenuated by dust in the disk of the galaxy, so again this object should move to the left in Fig 3R.

4 RESULTS FROM MAPS OF SELECTED SOURCES

Mapping data in the submillimetre from the SPIRE instrument (Griffin et al., 2010) on the *Herschel Space Observatory* (Pilbratt et al., 2010) is available for a few of the galaxies identified here as containing cold dust. This allows us to compare the location of the dust responsible for the submillimetre emission with the location of the starlight.

Two of the sources (NGC5701 and NGC5669) were observed as part of the *Herschel* Reference Survey (Boselli et al. 2010), and a third (NGC3049) was observed by the KINGFISH programme (Kennicutt et al. 2010). The SPIRE images were obtained from the *Herschel* or HerMES data archives.

For each of these objects we used an SDSS i band optical image to trace the optical surface brightness profile from stellar emission after smoothing by a gaussian matched to the size of the 250μm SPIRE beam, and then compared this to the 250μm surface brightness profile resulting from dust emission. The surface brightness profiles for this calculation
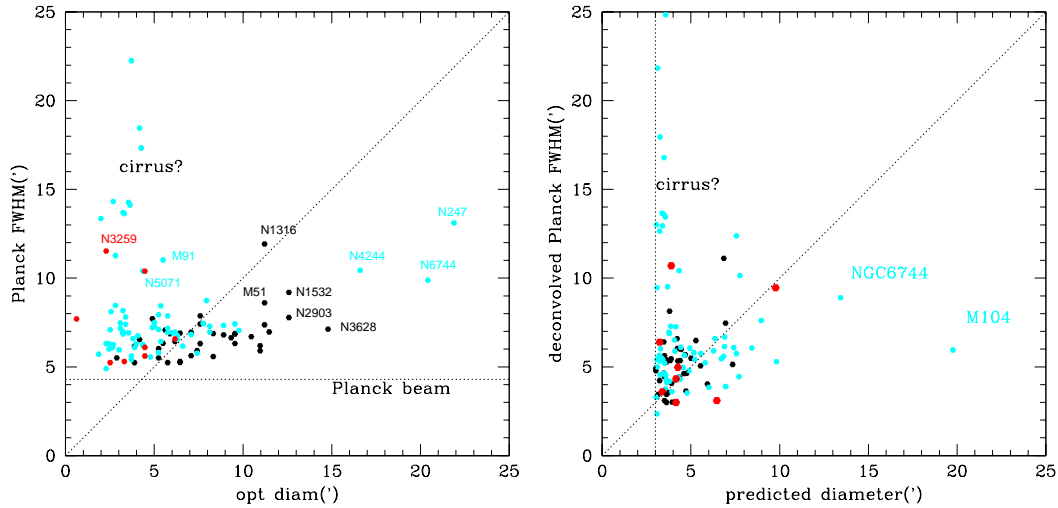
Figure 3. L: Observed *Planck* 857 GHz FWHM versus optical diameter (arcmins) for standard cirrus galaxies (ψ=5, black), cool cirrus galaxies (ψ=1, cyan) and cold cirrus galaxies (ψ=0.1, red). The dotted line denotes the Planck 857 GHz beam (FWHM). R: Deconvolved *Planck* 857 GHz FWHM versus predicted submillimetre diameter (arcmins) for standard cirrus galaxies (ψ=5, black), cool cirrus galaxies (ψ=1, cyan) and cold cirrus galaxies (ψ=0.1, red).

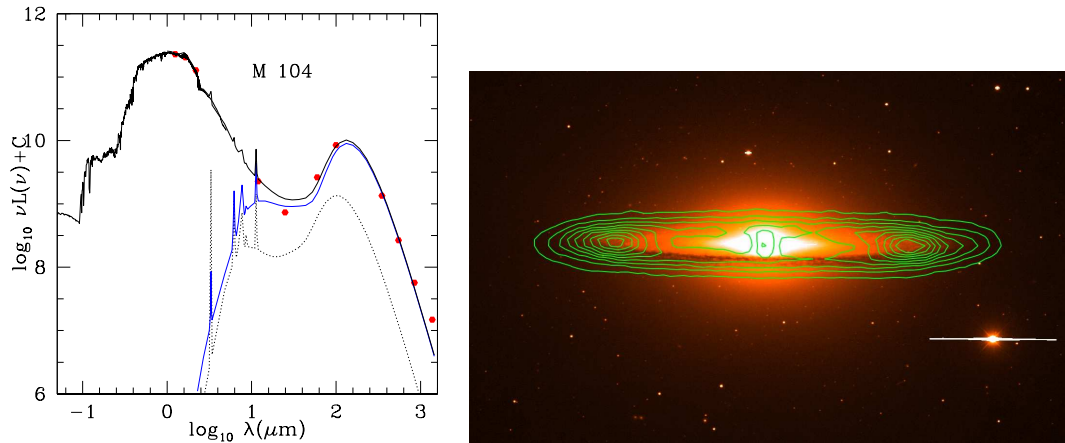Here the dotted line indicates the selection cutoff θ=3.0.

Figure 4. L: SED of M104, an outlier in Fig 3R. R: 250 μm contour map of M104 superposed on i-band image. Much of the 250 μm emission arises from a ring of dust outside the main optical image.

were produced using the the IRAF ellipse package and are plotted in Figs 6L and 7. In all cases the optical and submm surface brightness profiles are clearly different.

This is most obvious in NGC5701, where there is a large ring of cold dust located outside most of the optical light distribution (see Fig. 6R). This ring makes a substantial contribution to the integrated submm emission, but the optical emission from starlight in this region is much less than in the more central regions of this object.

The dust emission in NGC5669 has a larger scale length than the optical emission, with the ratio of submm to optical surface brightness rising all the way to the edge of detectable emission in this object. Examination of the optical image suggests that this dust is associated with extended low surface brightness optical emission away from the galaxy's nucleus and bright spiral arms.

NGC3049 is an edge on spiral, which makes this analy-sis a little less clear, and we see only a slight hint of changes to the optical to submm surface brightness ratio in the outer parts of this object, or possibly weak submm emission beyond the optically detected emission.

A further galaxy of interest, NGC1617, classified as cool in Table 2, was observed as part of the HerMES survey (Oliver et al., 2012) since it lies in the Akari Deep Field South (ADF-S, Matsuura et al 2011). Figure 9L shows 250 μm contours superposed on an r-band image (from Hameed and Devereux 1999), while Fig 9R shows 250 μm and r-band intensity profiles. In this case a significant fraction of the submillimetre emission arises from two dust blobs that lie along the major axis to the north-west.

Table 1. Galaxies requiring cold dust components

| IRAS name	z	L_{opt}	$log_{10}\theta_{pred}$	θ_{Planck}	$log_{10}\theta_{opt}$	ncirr	name
(a) *Planck* selected							
F10361+4155	0.002228	7.50	0.63	6.57	0.79	1	NGC3319
F14302+1006	0.00457	9.48	0.53	5.61	0.65	1	NGC5669
F09521+0930	0.00485	9.73	0.62	5.24	0.40	1	NGC3049
F10290+6517	0.00562	9.78	0.59	11.53	0.36	3	NGC3259
F14004+5603	0.00601	10.28	0.81	5.3	0.52	1	NGC5443
F15122+5841	0.00847	9.98	0.51	7.7	-0.21	3	MrK0847
F15248+4044	0.00874	10.20	0.62	6.1	0.65	1	UGC09858
F14366+0534	0.00502	10.48	0.99	10.39	0.65	3	NGC5701
F13405+6101	0.00732	9.70	0.43	6.71	0.23	1	UGC08684
F08233+2303	0.01794	9.97	-0.03				KUG0823+230B
F15243+5237	0.01948	10.63	0.36				UGC09853
F15495+5545	0.03974	10.90	-0.54				SBS1549+557
F04257-4913	0.05828	11.85	-0.10				ESO202-IG021
(b) RIFSCz selected							
F12234+3348	0.001060	8.25	0.550		1.12		NGC4395
F23461+0353	0.009860	10.02	0.466		0.40		NGC7757
F11555+2809	0.011230	10.15	0.475		0.26		NGC4004
F02533+0029	0.013820	10.59	0.604		0.15		UGC02403
F12208+0744	0.014160	10.01	0.304		0.36		NGC4334
F15097+2129	0.015700	10.42	0.464		0.18		UGC09763
F00342+2342	0.016110	10.35	0.418		0.43		NGC169 (Arp282)
F08070+3406	0.017520	10.92	0.666		0.35		NGC2532
F14280+2158	0.017750	10.24	0.321		0.19		UGC09316
F07581+3259	0.017910	10.38	0.387		-0.24		CGCG178-018
F08277+2046	0.020050	10.04	0.168		0.05		UGC04446
F09388+1138	0.020810	10.35	0.307		0.36		UGC05173
F13090+4658	0.027370	10.49	0.258		-0.23		UGC08269
F14236+0528	0.028400	10.38	0.187		-0.41		UGC09244
F23254+0830	0.028920	10.96	0.469		0.06		NGC7674
F08199+0427	0.028930	10.93	0.454		-0.31		CGCG032-009
F11078+0505	0.030230	10.69	0.315		-0.24		UGC06212
F15426+4115	0.031750	10.54	0.218		-0.05		NGC5992
F16269+4013	0.033570	10.30	0.074		-0.38		KUG1626+402
F14547+2449	0.033670	10.62	0.233		-0.18		UGC09618
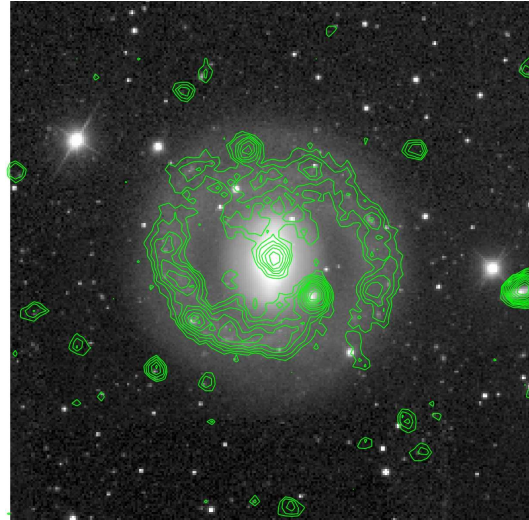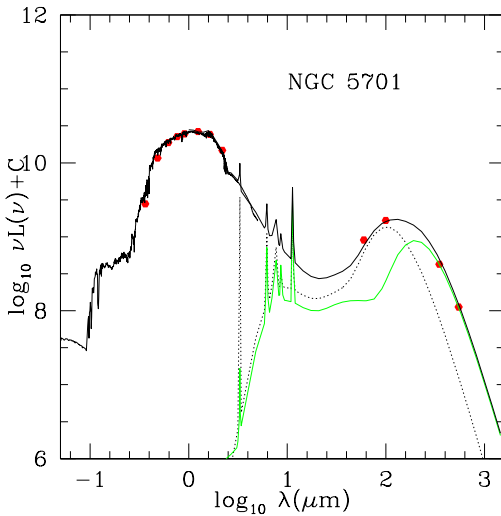
Figure 6. L: SED of NGC 5701. R: 250 μm map of NGC5701. In this case the submillimetre emission arises from a ring of dust lying outside the main stellar distribution. The peak of emission to the SW of the nucleus is a chance superposition of a background z=0.04 galaxy.

Table 2. Comparison samples of large galaxies requiring cool dust or normal cirrus components

IRAS name	z	L_{opt}	$log_{10}\theta_{pred}$	θ_{Planck}	$log_{10}\theta_{opt}$	ncirr	name
cool dust galaxies							
F00380-1408	0.005460	11.17	0.798	7.30	0.70	1	NGC0210
F00446-2101	0.000520	9.29	0.879	13.11	1.34	2	NGC0247
F01191+0459	0.007580	11.24	0.690	6.43	0.73	1	NGC0488
F01443+3519	0.015590	11.46	0.487	13.7	0.51	4	NGC0669
F02364+1037	0.011780	11.27	0.514	18.46	0.62	7	NGC1024
F02403+3707	0.001730	9.60	0.512	6.85	0.51	1	NGC1058
F02415-2912	0.004840	10.69	0.610	7.81	0.53	1	NGC1079
F03116-0300	0.005710	10.85	0.618	8.44	0.73	1	NGC1253
F03151-3245	0.015140	11.44	0.490	4.90	0.36	1	NGC1288
F03174-1935	0.005260	11.07	0.764	6.77	0.80	1	NGC1300
F03222-2143	0.005310	10.91	0.680	5.56	0.68	2	NGC1325
F03291-3348	0.006350	11.39	0.842	5.80	0.72	1	NGC1350
F03309-1349	0.006660	11.02	0.637	11.27	0.45	2	NGC1357
F03367-2629	0.004660	11.42	0.992	6.82	0.85	1	NGC1398
F03401-3003	0.005040	11.11	0.803	7.87	0.76	1	NGC1425
F03417-3600	0.004630	10.46	0.514	-9.99	0.47	5	NGC1436
F03451-3351	0.003600	10.37	0.579	6.00	0.39	2	IC1993
F04305-5442	0.003550	10.99	0.895	-9.99	0.63	5	NGC1617
F05452-3415	0.003070	10.50	0.713	7.22	0.69	1	NGC2090
F06209-5942	0.007560	10.89	0.516	7.40	0.53	161	ESO121-G026
F07184+8016	0.007350	11.39	0.779	5.77	0.87	2	NGC2336
F07525+6028	0.004810	10.62	0.578	8.11	0.41	3	NGC2460
F08547+0306	0.013080	11.32	0.493	6.59	0.58	1	NGC2713
F09076+0714	0.004500	11.18	0.887	6.19	0.64	3	NGC2775
F09134+7358	0.007540	11.04	0.593	5.61	0.57	3	IC0529
F09186+5111	0.002130	10.41	0.827	6.95	0.91	1	NGC2841
F10068-2849	0.003680	10.50	0.634	6.17	0.82	29	NGC3137
F10312-2711	0.011270	11.31	0.553	6.25	0.43	163	NGC3285
F10346-2718	0.009630	11.24	0.586	8.46	0.45	223	NGC3312
F10456-2034	0.013430	11.47	0.557	6.08	0.42	34	NGC3450
F11089-3636	0.008310	10.93	0.495	22.25	0.57	13	NGC3573
F11163+1321	0.002690	10.63	0.835	7.05	0.99	4	M065
F11549+5339	0.003500	11.04	0.926	7.44	0.89	2	M109
F12015+3210	0.002530	10.00	0.547	6.75	0.61	1	NGC4062
F12133+1325	0.000440	8.61	0.612	7.29	0.91	223	NGC4216
F12149+3805A	0.000810	9.05	0.567	10.44	1.22	1	NGC4244
F12194-3531	0.009790	11.12	0.519	6.99	0.51	6	ESO380-G019
F12234+1829	0.003070	10.04	0.483	5.41	0.57	11	NGC4394
F12257+2853	0.002210	9.87	0.541	6.30	0.60	1	NGC4448
F12259+1721	0.006520	11.06	0.666	7.10	0.72	3	NGC4450
F12329+1446	0.001620	10.30	0.890	11.02	0.74	2	M091
F12374-1120	0.003420	11.76	1.296	7.34	0.95	1	M104
F12407+0215	0.004450	10.69	0.647	7.47	0.49	2	NGC4643
F12415-4027	0.009850	11.19	0.552	14.12	0.56	5	NGC4650
F12474-1427	0.013060	11.41	0.539	6.31	0.36	5	MCG-02-33-017
F13191-3622	0.001560	10.39	0.952	8.74	0.90	2	NGC5102
F13331-3312	0.013990	11.37	0.489	-9.99	0.38	3	NGC5220
F13447-3041	0.014900	11.55	0.552	5.71	0.27	5	NGC5292
F13550-2904	0.008920	11.32	0.660	6.56	0.80	2	IC4351
F14134+3627	0.009590	11.12	0.528	6.96	0.79	2	NGC5529
F14424+0209	0.005750	11.36	0.870	7.45	0.89	2	NGC5746
F15045+0144	0.008530	10.99	0.514	6.26	0.64	2	NGC5850
F15110-1405	0.006640	11.03	0.643	6.09	0.59	1	NGC5878
F17304+1626	0.010400	11.24	0.553	25.21	0.49	1	NGC6389
F17576-6625	0.014480	11.56	0.569	-9.99	0.45	2	NGC6389
F18300-5832	0.007460	10.84	0.497	6.94	0.76	3	IC4721
F19049-6357	0.002800	11.25	1.128	9.88	1.31	2	NGC6744
F19101-6221	0.014490	11.50	0.539	14.27	0.55	3	IC4831
F19139-6035	0.012620	11.40	0.549	6.30	0.39	6	NGC6769
F19227-5503	0.010570	11.27	0.561	5.96	0.48	2	NGC6788
F19588-5613	0.014650	10.16	0.509	7.09	0.40	2	NGC6848
F20134-5257	0.009030	10.99	0.489	6.91	0.55	3	NGC6887
F20210-4348	0.009330	11.53	0.745	7.18	0.76	2	NGC6902
F20346-5217	0.015150	11.48	0.510	13.36	0.30	2	NGC6935

Table 3. Comparison samples of large galaxies requiring cool dust or normal cirrus components (cont.)

IRAS name	z	L_{opt}	$log_{10}\theta_{pred}$	θ_{Planck}	$log_{10}\theta_{opt}$	ncirr	name
cool dust galaxies (cont.)							
F20597-1700	0.004920	10.57	0.543	17.33	0.63	1	IC5078
F21029-4822	0.017200	11.63	0.529	14.32	0.43	3	ESO235-G057
F21142-6358	0.010490	11.21	0.534	6.9	0.51	4	IC5096
F21596-1909	0.008790	11.14	0.576	8.17	0.51	4	NGC7183
F21598-2103	0.008740	11.42	0.718	6.92	0.78	1	NGC7184
F22061-4724	0.005840	11.39	0.879	7.18	0.49	2	NGC7213
F22369-6644	0.010850	11.19	0.510	-9.99	0.59	1	NGC7329
F22450-2234	0.011140	11.56	0.683	-9.99	0.46	1	NGC7377
F22521-3955	0.005840	11.31	0.839	7.94	0.72	1	NGC7410
F22543-4339	0.005710	11.29	0.838	7.50	0.70	1	IC5267
F22544-4120	0.003130	10.48	0.694	7.42	0.98	1	NGC7424
F23105-2837	0.005220	10.60	0.532	13.64	0.52	1	NGC7513
F23120-4352	0.005320	10.80	0.624	-9.99	0.66	1	NGC7531
cirrus galaxies							
F01319-2940	0.004940	11.27	0.541	6.33	0.74	1	NGC0613
F02207-2127	0.005030	11.23	0.513	-9.99	0.78	1	NGC0908
F02441-3029	0.004240	11.41	0.678	6.32	0.98	4	NGC1097
F03075-2045	0.005350	11.44	0.592	5.92	0.87	1	NGC1232
F03207-3723	0.005870	12.01	0.836	11.92	1.05	4	NGC1316
F03316-3618	0.005460	11.57	0.648	7.37	1.05	2	NGC1365
F03404-4722	0.003590	11.03	0.560	6.9	0.81	2	NGC1433
F04022-4329	0.002990	10.87	0.559	6.8	0.95	1	NGC1512
F04101-3300	0.003470	11.04	0.580	9.2	1.10	1	NGC1532
F04188-5503	0.005020	11.34	0.569	5.58	0.92	8	NGC1566
F04449-5920	0.004440	11.18	0.543	6.88	0.92	117	NGC1672
F05035-3802	0.004040	11.13	0.559	5.51	0.72	2	NGC1792
F07365-6924	0.004890	11.27	0.546	5.3	0.81	7	NGC2442
F08491+7824	0.004670	11.22	0.541	7.71	0.69	4	NGC2655
F08495+3336	0.001370	10.36	0.643	6.87	0.98	1	NGC2683
F09293+2143	0.001830	10.77	0.723	7.78	1.10	4	NGC2903
F10126+7338	0.009350	11.86	0.559	5.24	0.59	1	NGC3147
F10407+2511	0.001930	10.55	0.589	6.95	0.85	1	NGC3344
F10413+1157	0.002590	10.88	0.627	7.41	0.88	3	M095
F10441+1205	0.002990	11.08	0.664	6.31	0.88	3	M096
F11032+0014	0.002670	11.20	0.773	5.9	1.04	7	NGC3521
F11176+1315	0.002430	11.06	0.744	6.64	0.97	2	M066
F11176+1351	0.002810	11.04	0.671	7.13	1.17	4	NGC3628
F12006+4448	0.002340	10.56	0.511	6.03	0.72	1	NGC4051 Seyf1
F12163+1441	0.008030	11.70	0.545	7.08	0.75	222	M099
F12193+0445	0.005220	11.43	0.597	5.25	0.81	7	M061
F12203+1605	0.005240	11.49	0.626	7.87	0.88	33	M100
F12239+3130	0.002390	10.63	0.537	-9.99	0.56	2	NGC4414
F12294+1441	0.007610	11.91	0.674	5.63	0.85	4	M088
F12334+2814	0.002690	10.75	0.545	6.19	1.04	1	NGC4559
F12410+1151	0.004700	11.14	0.498	5.51	0.46	3	NGC4647 (or 0.85 M60?)
F12464-0823	0.004650	11.41	0.638	6.17	0.59	3	NGC4699
F12498-0055	0.004130	11.20	0.584	6.87	0.77	1	NGC4753
F12542+2157	0.001360	10.80	0.866	6.7	1.02	3	M064
F13086+3719	0.003160	11.03	0.615	5.24	0.76	2	NGC5005
F13170-2708	0.007230	11.48	0.481	6.54	0.62	1	NGC5078
F13277+4727	0.001540	10.86	0.842	8.61	1.05	5	M051a
F13350+0908	0.003840	10.93	0.481	6.43	0.79	1	NGC5248
F22347+3409	0.002720	11.07	0.700	6.97	1.06	53	NGC7331
F23552-3252	0.000770	9.83	0.629	6.85	0.98	1	NGC7793

5   DISCUSSION AND CONCLUSIONS

The analysis of *Planck* 350 μm data shows very clearly that the galaxies whose SEDs require a cold dust component are indeed larger than normal galaxies and by an amount consistent with the interpretation that the surface bright-ness of the illuminating starlight is lower. The fact that this phenomenon of galaxies with cold dust did not show up in follow-up of IRAS galaxies refelects the fact that 60 μm se-lection biases samples towards galaxies with warmer dust. It needed the submillimetre sensitivity of *Herschel* and *Planck* to uncover this phenomenon.
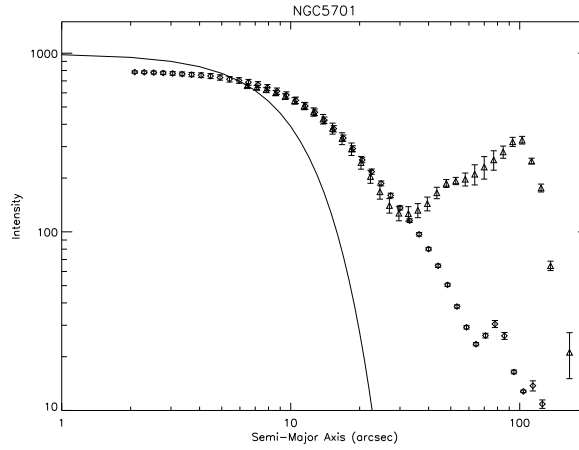
Figure 7. 250 μm and optical intensity profiles of NGC5701. Diamonds indicate the i band surface brightness derived from an SDSS image after it has been smoothed by a gaussian matching the SPIRE beam at 250μm, triangles show the 250μm surface brightness from SPIRE observations. The solid line indicates a gaussian model of the SPIRE 250μm beam as given by the SPIRE Handbook http://herschel.esac.esa.int/Docs/SPIRE/spire_handbook.pdf. The true Herschel beam at 250μm deviates somewhat from a pure Gaussian at radii beyond $\sim$ 20 arcsecondsm at levels < a few percent (Griffen et al. 2013). This is insignificant to the current analysis. The surface brightness scale is arbitrary with the two profiles scaled to the same value at a semi-major axis radius of 10 arcseconds In this case strong submillimetre emission arises in a ring of dust lying outside the main stellar distribution, which can be seen in Fig. 6R, leading to a region where the optical-to-submilimetre ratio is low.
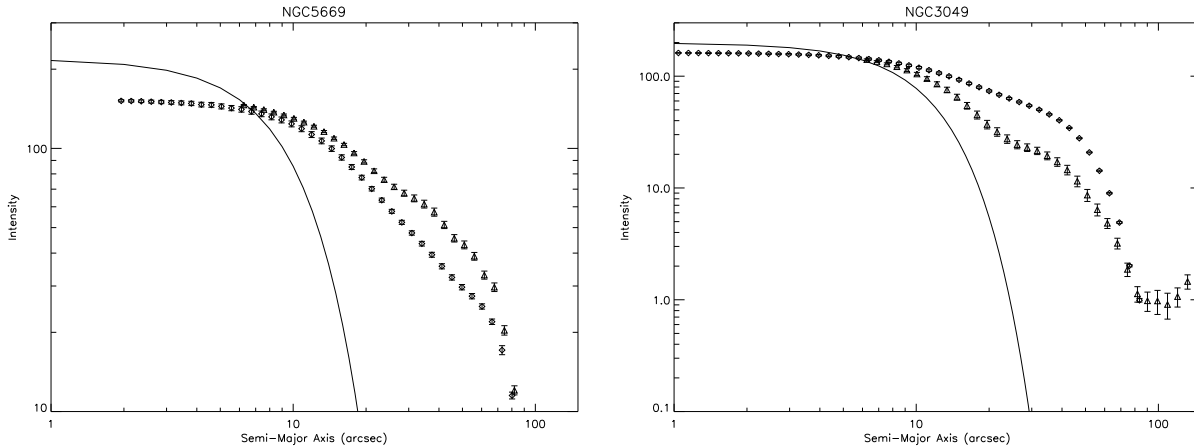
Figure 8. L: 250 μm and optical intensity profiles of NGC5669. Symbols and scalings as in Fig. 6R. R: 250 μm and optical intensity profiles of NGC3049. Symbols and scalings as in Fig. 6R.

The limited submillimetre mapping data available for these cold dust galaxies shows that a variety of geometries may be involved. NGC5701 shows a large ring of cold dust located outside most of the optical light distribution but in NGC3049 the cold dust appears to be located closer to the centre of the galaxy.

It is unlucky that none of our cold dust galaxies is in the sample of nearby galaxies for which Bendo et al (2015) have studied the 160/250 and 250/350 μm surface brightness profiles in detail. The next step will be to map some of these cold dust galaxies with ground-based submillimetre telescopes.
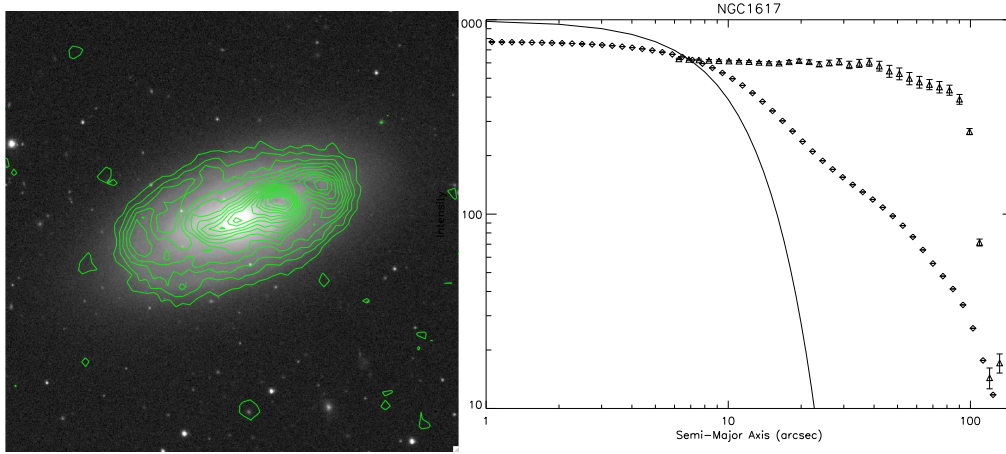
6 ACKNOWLEDGEMENTS

Figure 9. L: 250 μm contours of NGC1617 superposed on r-band image. R: 250 μm and optical intensity profiles of NGC1617. Symbols and scalings as in Fig. 6R.

REFERENCES

Ade P.A.R. et al, 2011, Planck early results XVI, AA 536, 16
Bendo G.J. et al, 2015, MNRAS 448, 135
Boselli A. et al, 2010, PASP 122, 261
Bourne N. et al, 2013, MNRAS 436, 479
Efstathiou A., Rowan-Robinson M., 2003, MNRAS 343, 322
Efstathiou A., Rowan-Robinson M., Siebenmorgen R., 2000, MNRAS 313, 734
Galametz M. et al, 2012, MNRAS 425, 763
Griffin M.J. et al, 2010, AA 518, L3
Griffin M.J. et al, 2013, MNRAS 434, 992
Hameed S., Devereux N., 1999, AJ 118, 730
Ibar E. et al, 2013, MNRAS 449, 2498
Kennicutt R.C. et al, 2010, PASP 123, 1347
Pilbratt G. et al, 2010, AA 518, L1
Rice W., Lonsdale C.J., Soifer B.T., Neugebauer G., Kopan E.L., Lloyd L.A., de Jong T., Habing H.J., 1988, ApJS 68, 91
Rowan-Robinson M., 1992, MNRAS 258, 787
Rowan-Robinson M. et al, 2005, AJ 129, 1183
Rowan-Robinson M. et al, 2008, MNRAS 386, 697
Rowan-Robinson M. et al, 2010, MNRAS 409, 2
Rowan-Robinson M. et al, 2013, MNRAS 428, 1958
Rowan-Robinson M. et al, 2014, MNRAS 445, 3848
Smith D.J.B. et al, 2012, MNRAS 427, 703
Symeonidis M. et al, 2013, MNRAS 431, 2317
Wang L., Rowan-Robinson M., 2009, MNRAS 398, 109
Wang L., Rowan-Robinson M., Norberg P., Heinis S., Han J., 2014, MNRAS 442, 2739